AIAA JOURNAL
Vol. 55, No. 3, March 2017

Low-Probability Events Leading to Rocket Engine Combustion Instability

Pavel P. Popov,* Athanasios Sideris,† and William A. Sirignano‡
University of California, Irvine, Irvine, California 92697

DOI: 10.2514/1.J055276

A new method is proposed for calculations of rare-event rocket combustion instabilities. Acceleration of the combustion chamber is modeled as a stochastic process of long duration and moderate amplitude. Using a simplified model for the effect of acceleration on the evolution of the first tangential mode of pressure within the chamber, a modified sampling distribution is obtained that yields higher occurrence of the rare event: in this case, growth to instability. Statistics are then calculated for the original distribution of the stochastic process using an importance sampling procedure. Knowledge of the likelihood ratios between the real and modified probability density functions allows a low-cost computation of the probability of the rare event of triggering the combustion instability by low-amplitude acceleration fluctuations. There are two distinct regimes of high and low probabilities of triggering, with a critical acceleration amplitude threshold between them; in the low-probability regime, the probability of triggering increases exponentially with increasing acceleration amplitude. The probability of triggering increases with increasing duration of the stochastic acceleration. This method of low-probability event analysis can be extended to other instability-triggering mechanisms.

Downloaded by UC IRVINE on March 15, 2017 | http://arc.aiaa.org | DOI: 10.2514/1.J055276

Nomenclature

a	=	speed of sound, m/s
$\boldsymbol{a}$	=	sample space variable for acceleration, m/s^2
a_0	=	expected root mean square of acceleration, m/s^2
$\boldsymbol{a}^C$	=	continuous acceleration history, m/s^2
C	=	constant used in Eq. (2)
E	=	rate of heat release, W/m^3
F	=	inertial force, N
j	=	imaginary unit; $\sqrt{-1}$
$\boldsymbol{m}_i$	=	modified mean for acceleration probability density function, m/s^2
P_L	=	cumulative likelihood ratio
p	=	pressure, N $\cdot$ m^{-2}
p_i	=	discrete likelihood ratios
R	=	chamber radius, m
t	=	time, s
u_j	=	Cartesian velocity component, m/s
γ	=	ratio of specific heats
ρ	=	gas density, k
σ_0	=	power spectral density of ideal white noise acceleration

Subscripts

i	=	index for time step
j	=	index for Cartesian coordinates
O	=	oxidizer
0	=	undisturbed state

Presented as Paper 2016-1932 at the 54th AIAA Aerospace Sciences Meeting, San Diego, CA, 4–8 January 2016; received 12 April 2016; revision received 29 July 2016; accepted for publication 2 August 2016; published online 19 January 2017. Copyright © 2016 by Pavel P. Popov, Athanasios Sideris and William A. Sirignano. Published by the American Institute of Aeronautics and Astronautics, Inc., with permission. All requests for copying and permission to reprint should be submitted to CCC at www.copyright.com; employ the ISSN 0001-1452 (print) or 1533-385X (online) to initiate your request. See also AIAA Rights and Permissions www.aiaa.org/randp.

*Postdoctoral Researcher, Department of Mechanical and Aerospace Engineering.
†Professor, Department of Mechanical and Aerospace Engineering.
‡Professor, Department of Mechanical and Aerospace Engineering. Fellow AIAA.

I. Introduction

THIS work addresses the problem of liquid-propellant rocket engine (LPRE) instability: a well-known rocket engine phenomenon in which the high-energy release of combustion reinforces acoustic waves within the combustion chamber to a destructive amplitude. The dynamics of LPRE instability are highly nonlinear and challenging to predict [1,2] but, nevertheless, each new rocket engine design requires that this potential mode of failure be prevented [3].

Two main types of LPRE instabilities are known to occur. In "chugging" instability [4], the pressure distribution within the combustion chamber is spatially uniform but varies with time. This type of low-frequency instability is driven by the coupling between the mean pressure and the propellant mass flux: as such, it can be counteracted by the introduction of damping elements in the injector feed system. Screeching instability, on the other hand, occurs when an acoustic wave from one of the dominant resonant modes of the combustion chamber receives energy from the combustion heat release and increases to a destructive amplitude [5]. As this is a phenomenon that occurs mainly within the combustion chamber, its prevention is more difficult, usually involving the use of baffles within the combustion chamber, which decrease performance, or fine tuning of the injector configuration [3] that, when done experimentally, requires costly design iterations. Therefore, there is strong motivation for the development of simulation tools for the analysis of screeching instability. For LPRE combustion instability, the oscillations are acoustical, although highly nonlinear. In other combustors for solid rockets, ramjets, and gas turbines, a combination of acoustic and kinematic wave propagation can occur. The wave traveling in the downstream direction might be kinematic, i.e., moving with the material. Common examples are vortex structures and short-wavelength entropy (or temperature and composition) undulations. These can be reflected as acoustic waves that travel upstream to regions of injection and/or combustion; there, they can cause another kinematic wave to form and propagate downstream. A cyclic behavior can occur. These are uncommon in LPREs, and they are inherently of lower amplitude and less negative consequence compared to fully acoustic oscillations. They will not be considered here. Nevertheless, vorticity and entropy variation are essential in the combustion process. The turbulent combustion models in previous analyses [2,6–9] consider these matters. The wave propagation is primarily an irrotational process, weakly modified by the rotational effects that occur on length scales much smaller than the acoustic wavelength, i.e., the transverse dimensions of individual coaxial injectors or wall boundary-layer thicknesses. Our model

takes advantage of this fact by considering the wave dynamics to be irrotational. The main mechanism for damping of LPRE instabilities has long been known to be caused by nozzle outflow of acoustical energy [1,10,11]. The nozzle-damping physics are most clearly quantified by a perturbation scheme [12]; although, of course, it is represented in the computational fluid dynamics (CFD) models. That primary effect remains in our model.

In previous studies, we considered various types of disturbances that occurred at operating conditions wherein the LPRE was stable to small-amplitude disturbances. That is, below some threshold disturbance, the engine returned to steady-state operation; whereas above the threshold, the oscillation was triggered and grew to a limit cycle. The studied disturbances had short durations on the order of the period of oscillation for a resonant acoustic mode. However, we know the following from simple oscillatory systems, such as a mass with spring or a pendulum. An oscillation can be forced to a limit-cycle oscillation with a single pulse of sufficient magnitude. Or, many small pulses, properly organized over a longer duration, can yield the same result. Proper organization is a key concept: if the many small disturbances are random, cancelations due to phase differences and directional differences are highly likely and development to a limit cycle is highly unlikely. Nevertheless, there is a small chance that the random forcing becomes proper and a limit-cycle results. In this paper, we address this low-probability triggering for LPRE triggering.

There are multiple types of disturbances that can trigger screeching combustion instability, such as disruptions in the propellant injection process, shedding in the combustion chamber of large rogue vortices that eventually flow through the choked nozzle [13], significant fluctuations in local burning rates [6,7], or an acceleration of the entire LPRE [6]. In all of these studies, the limit cycle of the observed acoustic instability was independent of the triggering event, and it had the shape of a first tangential acoustic mode for the cylindrical combustion chamber. In this work, we extend the analysis of acceleration-caused instability by considering prolonged acceleration disturbances of a stochastic nature; again, when an acoustic instability develops, its limit cycle has the shape of a first tangential acoustic mode for the cylindrical combustion chamber.

The main goal is to estimate the probability of occurrence of rare events, such as the development of an acoustic instability in a rocket engine that is subjected to a period of random acceleration of relatively low amplitude. Previously, it has been established [8,9] that a short [$O(1\text{ ms})$] acceleration pulse of high amplitude [$O(2000\text{ m/s}^2)$] was capable of triggering an acoustic instability, provided its frequency matched the acoustic frequency of the combustion chamber. Another likely trigger of instability would be a longer [$O(20\text{ ms})$] acceleration pulse of lower amplitude [$O(100\text{ m/s}^2)$]: this acceleration disturbance was modeled as a smooth stochastic process with a fixed mean rms amplitude a_{τ_F} [see Eq. (14)]. Such an acceleration history may come about due to the random nature of the aerodynamic forces acting on the rocket. The question to answer is the following: If the acceptable likelihood of instability development is very low, such as $1/10{,}000$, at what level of the mean rms amplitude a_{τ_F} is this probability exceeded? An additional question of interest is which realizations of the stochastic process lead to an instability, as well as what they have in common.

Because we are interested in the estimation of very rare stochastic events, a straightforward Monte Carlo simulation is computationally inefficient: estimating the actual probability of a random event at the 95% confidence level, when that probability is on the order of magnitude of $1/10{,}000$, would require approximately four million samples. To overcome this obstacle, we use the importance sampling method [14] to perform variance reduction. Importance-sampling-based variance reduction is a well-known tool for rare-event simulation, which found wide application in economics to problems such as credit portfolio risk assessment [15–18], as well as in signal processing [19], when particle filtering is required. The present work serves in part to demonstrate the effectiveness of this approach to the field of computational fluid dynamics for problems that require the analysis of statistical outliers.

II. Governing Equations

This study considered a 10-injector cylindrical rocket engine, which was previously shown to be conditionally unstable, with a limit-cycle instability that could be triggered by a preexisting pressure wave [2], a pressure pulse [7], an injector blockage [6], or a whole-body acceleration of the combustion chamber [8], which is the disturbance considered here. Only transverse acceleration and first-tangential-mode instability will be considered in this work. The combustion chamber is a cylinder for which the length is $L = 0.5$ m and for which the radius is $R = 0.14$ m, with the injectors distributed in three rings: with one injector at the center of the chamber, three injectors at a radius of $r = R/2$, and the remaining six injectors spread evenly at a radius of $r = 3R/4$ from the center (see Fig. 1).

Each injector consists of two concentric ports, the inner of which serves as the oxidizer port and has a radius of 0.898 cm; the outer, annular port has an inner radius of 0.898 cm and an outer radius of 1.1 cm, and it serves as the fuel inlet. Both fuel and oxidizer injector ports have lengths of 11.5 cm. For this case, the fuel is methane (CH_4), the oxidizer is liquid oxygen (LOX), and the mean pressure inside the combustion chamber at standard operating conditions is 200 atm. For more details of this computational configuration, the reader is referred to the work of Sirignano and Popov [2], and Popov et al. [6]. This computational algorithm has previously been compared to existing experimental data [9,20,21] and found to accurately predict single instances of instability onset at low computational cost: in this work, we build on this algorithm by coupling it to a Monte Carlo simulation framework with a variance reduction strategy.

Here, we solve for pressure and velocity in a reference frame fixed to the combustion chamber, which undergoes irrotational acceleration $\boldsymbol{a}^C(t)$. Therefore, in the accelerating frame, the fluid experiences the inertial force

$$F_i = -\rho \boldsymbol{a}^C(t) \tag{1}$$

Following Popov et al. [8], with the inclusion of this inertial force, the momentum equation for the combustion chamber becomes the following:

$$\frac{\partial u_i}{\partial t} + u_j \frac{\partial u_i}{\partial x_j} + \frac{C}{p^{1/\gamma}} \frac{\partial p}{\partial x_i} + a_i^C = 0 \tag{2}$$

and the wave equation governing the evolution of pressure is as follows:

$$\frac{\partial^2 p}{\partial t^2} - a^2 \frac{\partial^2 p}{\partial x_j \partial x_j} = \frac{\partial \rho}{\partial t}\frac{\partial a^2}{\partial t} + (\gamma - 1)\frac{\partial E}{\partial t} + a^2 \frac{\partial^2 (\rho u_j u_i)}{\partial x_i \partial x_j} + a^2 \frac{\partial \rho}{\partial x_i} a_i^C \tag{3}$$

The inertial force also modifies the pressure boundary condition at the chamber walls, for which the form is

$$\frac{\partial p}{\partial n} = \frac{p^{1/\gamma} u_t^2}{C R_c} - \frac{p^{1/\gamma} a_n^C}{C} \tag{4}$$

where u_t is the velocity component tangential to the boundary; R_c is the wall boundary radius of curvature; and n and a_n^C are, respectively, the unit outward normal vector at the boundary and the component of the acceleration in that direction.

III. Importance Sampling for Low-Probability Event Estimation

In this work, the acceleration disturbance $\boldsymbol{a}^C(t)$ is modeled as a smoothed white noise (the derivative of a Wiener process) applied for t_d s. Thus, we take $\boldsymbol{a}^C(t)$ to be a continuously differentiable random process defined by a discrete sequence $\boldsymbol{A}_i$ of random vectors that set the value of $\boldsymbol{a}^C(t)$ at discrete points in time t_i, $i = 0, 1, \ldots, N-1$. The time points t_i are uniformly distributed with spacing determined

Downloaded by UC IRVINE on March 15, 2017 | http://arc.aiaa.org | DOI: 10.2514/1.J055276

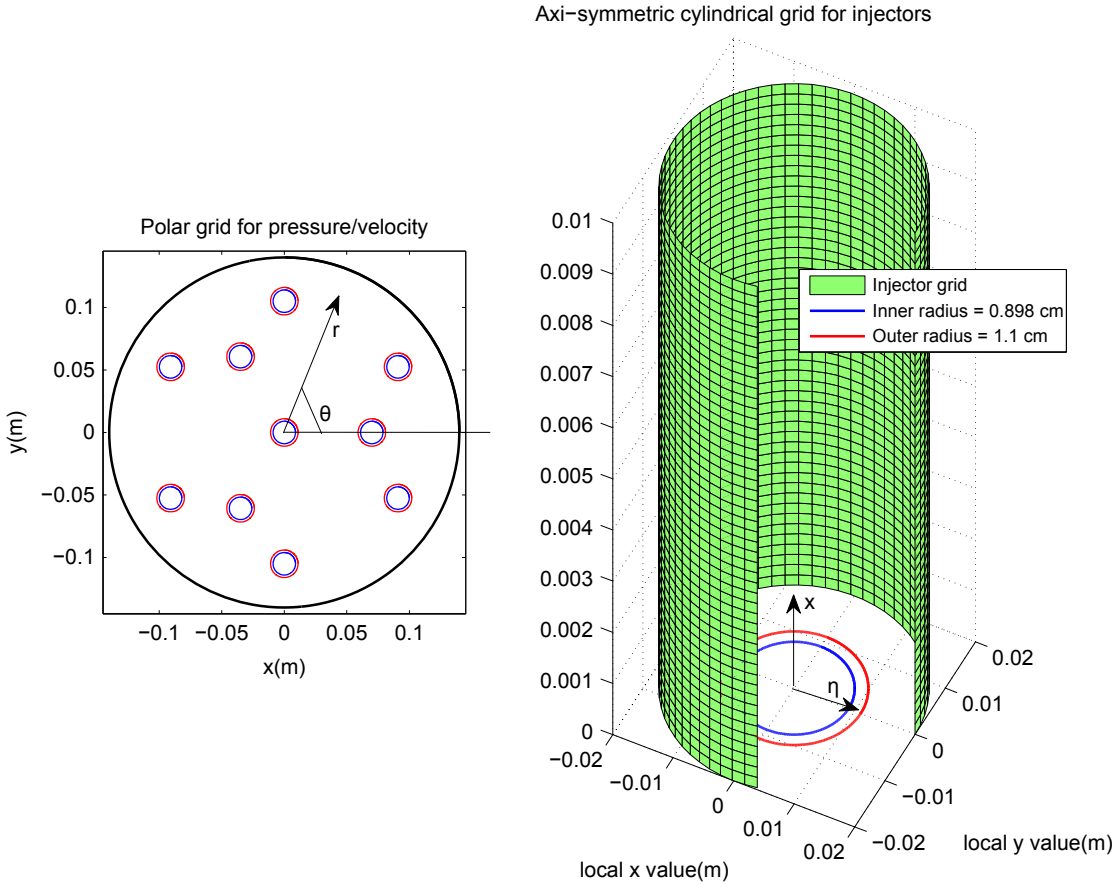

Fig. 1 Cylindrical combustion chamber and injector distribution (left), and axisymmetric cylindrical grid used for the solution of each of the 10-injector jet flames (right).

by a parameter $t_s = t_{i+1} - t_i$. Therefore, $N = t_d/t_s$. More specifically, for $i = 0, 1, \ldots, N-1$,

$$\boldsymbol{a}^C(t_i = i \times t_s) = \boldsymbol{A}_i \tag{5}$$

$$\boldsymbol{a}^C(t_{i+1} = (i+1) \times t_s) = \boldsymbol{A}_{i+1} \tag{6}$$

$$\boldsymbol{a}^C(t_i < t < t_{i+1}) = \cos^2\left(\frac{\pi(t-t_i)}{2t_s}\right)\boldsymbol{A}_i + \sin^2\left(\frac{\pi(t-t_i)}{2t_s}\right)\boldsymbol{A}_{i+1} \tag{7}$$

The random variables $\boldsymbol{A}_i$ are independent and identically distributed, sampled from a two-dimensional uniform Gaussian distribution $\mathsf{N}(0, \sigma^2)$ with a mean of zero and a standard deviation of σ. A straightforward calculation shows that σ relates to the root-mean-square (rms) value of the one-dimensional disturbance $a_x^C(t)$ (say, along the x axis) via the simple equation

$$a_0 \equiv \sqrt{\frac{1}{t_d}E\left[\int_0^{t_d}(a_x^C(t))^2\,\mathrm{d}t\right]} = \frac{\sqrt{3}}{2}\sigma \tag{8}$$

In Eq. (8), the expectation $E[\cdot]$ is taken with respect to $\boldsymbol{A}_i$.

For the disturbance signal $a^C(t)$ to approximate a white noise process as $t_s \to 0$, it is necessary for σ to satisfy the scaling law

$$\sigma = \frac{\sigma_0}{\sqrt{t_s}} \tag{9}$$

where σ_0 is a constant. The scaling law [Eq. (9)] should be expected: as is well known, a Wiener process, discretized over time steps of length t_s, requires increments proportional to $\sqrt{t_s}$ in order for its autocorrelation over a fixed time level (such as the period of the first tangential mode $\tau_F = 0.453$ ms) to converge as we take $t_s \to 0$. Because we are approximating the derivative of a Wiener process, the correct level of the random vectors is $\sigma = \text{const}(\sqrt{t_s}/t_s)$, which leads to $\sigma^2 t_s = \text{const.}$ in order to get convergence (in the weak sense, when we integrate over a given time interval). In the Appendix, we show analytically that $a_x^C(t)$ converges to white noise under the scaling law [Eq. (9)] as $t_s \to 0$ by explicitly computing the power spectral density (PSD) $\mathsf{S}_a(\omega)$ of $a_x^C(t)$. $\mathsf{S}_a(\omega)$ is a description of the power of $a_x^C(t)$ versus frequency and is defined via the Fourier transform $\mathsf{A}_x(j\omega)$ of $a_x^C(t)$, truncated in $[0t_d]$ as

$$\mathsf{S}_a(\omega) = \lim_{t_d \to \infty}\frac{1}{t_d}E[|\mathsf{A}_x(j\omega)|^2] \tag{10}$$

More specifically, we derive the exact expression

$$\mathsf{S}_a(\omega; t_s) = \frac{2\sigma_0^2}{t_s^2}\left[\frac{\pi^2}{2\omega(\omega^2 t_s^2 - \pi^2)}\right]^2(1 - \cos(2\omega t_s)) \tag{11}$$

(where we explicitly denote the dependence of the power spectral density on t_s) and show that

$$\mathsf{S}_a(\omega; t_s = 0) \equiv \lim_{t_s \to 0}\mathsf{S}_a(\omega; t_s) = \sigma_0^2 \tag{12}$$

Therefore, $a_x^C(t)$ indeed approximates a white noise process because white noise can be equivalently defined as a stochastic signal for which the power spectral density is constant [22]. The parameter σ_0 defines the power spectrum of the white noise signal approximated by $a_x^C(t)$ and appears as a natural parameter that characterizes the disturbance. Notice that a_0, the actual average power of $a_x(t)$, from Eqs. (8) and (9) increases to ∞; as $t_s \to 0$, as it should because a pure

Downloaded by UC IRVINE on March 15, 2017 | http://arc.aiaa.org | DOI: 10.2514/1.J055276

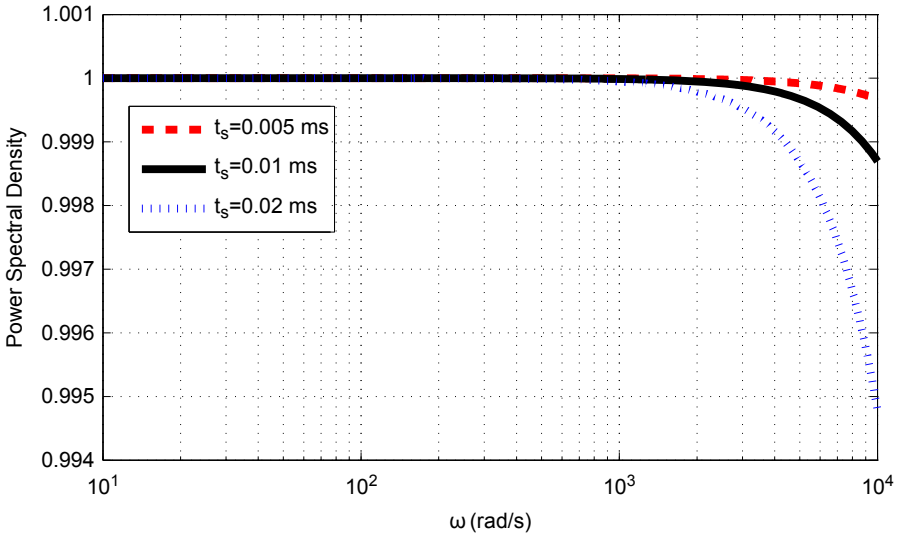

Fig. 2 Power spectral density of the disturbance signal a_x^C for sampling intervals of t_s 0.05, 0.01, and 0.02 ms.

Downloaded by UC IRVINE on March 15, 2017 | http://arc.aiaa.org | DOI: 10.2514/1.J055276

white noise signal has infinite power. However, we can interpret σ_0 as an rms acceleration through Eqs. (8) and (9) by using a nominal t_s such as τ_F. Namely, we introduce the equivalent parameter

$$a_{\tau_F} \equiv \frac{\sqrt{3}}{2}\frac{\sigma_0}{\sqrt{\tau_F}} \tag{13}$$

and further results will be expressed in terms of a_{τ_F}. In particular,

$$\boldsymbol{A}_i \sim \frac{1}{2\pi(4\tau_F/3t_s)a_{\tau_F}^2}\exp\left(-\frac{\|\boldsymbol{a}-0\|^2}{(8\tau_F/3t_s)a_{\tau_F}^2}\right) \tag{14}$$

where the preceding formula reads as "$\boldsymbol{A}_i$ is distributed accordingly to the following probability density function (PDF)"; and the reader should not be surprised that the right-hand side has units of inverse acceleration because a PDF has the inverse units of its sample space.

Figure 2 plots the PSD $\mathsf{S}_a(\omega; t_s)$ normalized by σ_0^2 for different values of t_s. It is seen that the adopted disturbance model [Eq. (7)] constitutes essentially a band-limited white noise model. As discussed in Sec. IV, the disturbances that tend to cause triggering exhibit strong energy content around the first-tangential-mode frequency. Therefore, it is expected that the probability of triggering is not affected significantly by the choice of t_s. provided that $(2\pi t_s)/\tau_F \ll 1$ and the disturbance signal behaves as band-limited white noise for the first-tangential-mode frequency. In the following, we fix $t_s = 0.01$ ms. This choice provides a reasonable compromise between more closely approximating pure white noise (by taking t_s to be small in comparison with the period of the first tangential mode, $\tau_F = 0.453$ ms) and preserving the smoothness of the acceleration $\boldsymbol{a}^C$ in relation to the simulation time step $dt = 2.5 \times 10^{-7}$ s. Indeed, for $t_s = 0.01$ ms, the relative error

$$|\mathsf{S}_a(\omega; t_s) - \mathsf{S}_a(\omega; t_s = 0)|/\mathsf{S}_a(\omega; t_s = 0)$$

at the first-tangential-mode frequency $\omega_F = 2\pi/\tau_F = 13.87 \times 10^3$ rad/s is 0.25%. It is also interesting that the relative error is independent of σ_0^2. This is also established numerically for the values $t_s = 0.02$ ms and $t_s = 0.005$ ms (see Table 1 in Sec. IV) in support of the previous analysis.

The idea of the present importance sampling approach to variance reduction [14] is to generate the sequence $\boldsymbol{A}_i$ using a probability distribution $\mathsf{N}(\boldsymbol{m}_i, \sigma^2)$, with $\boldsymbol{m}_i$ selected as explained in the following text, as a function of the solution at $t = t_{i-1}$ so that the oscillation amplitude will tend to increase.

Therefore, we set

$$\boldsymbol{A}_i \sim \frac{1}{2\pi(4\tau_F/3t_s)a_{\tau_F}^2}\exp\left(-\frac{\|\boldsymbol{a}-\boldsymbol{m}_i\|^2}{(8\tau_F/3t_s)a_{\tau_F}^2}\right) \tag{15}$$

And, because the distributions in Eqs. (14) and (15) have the same support (namely, the entire plane), samples taken using the modified distribution (with mean $\boldsymbol{m}_i$) can be used to calculate statistics for the original distribution [see Eq. (20)].

More specifically, the target PDF, $P_{\text{target}}(\boldsymbol{A}_1, \boldsymbol{A}_2, \ldots, \boldsymbol{A}_N)$, of getting a particular string of vectors $\{\boldsymbol{A}_1, \boldsymbol{A}_2, \ldots, \boldsymbol{A}_N\}$ in our stochastic calculations is given by

$$P_{\text{target}}(\boldsymbol{A}_1, \boldsymbol{A}_2, \ldots, \boldsymbol{A}_N) = \prod_i \frac{1}{2\pi(4\tau_F/3t_s)a_{\tau_F}^2}\exp\left(-\frac{\|\boldsymbol{A}_i-0\|^2}{(8\tau_F/3t_s)a_{\tau_F}^2}\right) \tag{16}$$

On the other hand, as $\boldsymbol{m}_i$ is a function of $\{\boldsymbol{A}_1, \boldsymbol{A}_2, \ldots, \boldsymbol{A}_{i-1}\}$, we have that the modified sample PDF, $P_{\text{modified}}(\boldsymbol{A}_1, \boldsymbol{A}_2, \ldots, \boldsymbol{A}_N)$, of getting a particular string of vectors $\{\boldsymbol{A}_1, \boldsymbol{A}_2, \ldots, \boldsymbol{A}_N\}$, is as follows:

$$\begin{aligned} &P_{\text{modified}}(\boldsymbol{A}_1, \boldsymbol{A}_2, \ldots, \boldsymbol{A}_N) \\ &\quad = P(\boldsymbol{A}_1)P(\boldsymbol{A}_2|\boldsymbol{A}_1)\ldots P(\boldsymbol{A}_N|\boldsymbol{A}_1, \boldsymbol{A}_2, \ldots, \boldsymbol{A}_{N-1}) \\ &\quad = \prod_i \frac{1}{2\pi(4\tau_F/3t_s)a_{\tau_F}^2}\exp\left(-\frac{\|\boldsymbol{A}_i-\boldsymbol{m}_i\|^2}{(8\tau_F/3t_s)a_{\tau_F}^2}\right) \end{aligned} \tag{17}$$

because Eq. (15) implies that, provided $\boldsymbol{m}_i$ is a unique function of $\{\boldsymbol{A}_1, \boldsymbol{A}_2, \ldots, \boldsymbol{A}_{i-1}\}$, then

$$P(\boldsymbol{A}_i|\boldsymbol{A}_1, \boldsymbol{A}_2, \ldots, \boldsymbol{A}_{i-1}) = \frac{1}{2\pi(4\tau_F/3t_s)a_{\tau_F}^2}\exp\left(-\frac{\|\boldsymbol{A}_i-\boldsymbol{m}_i\|^2}{(8\tau_F/3t_s)a_{\tau_F}^2}\right) \tag{18}$$

Table 1 Comparison between probabilities of growth to instability for different values of t_s

	$t_s = 0.005$ ms, mean probability	$t_s = 0.005$ ms, CI width	$t_s = 0.01$ ms, mean probability	$t_s = 0.01$ ms, CI width	$t_s = 0.02$ ms, mean probability	$t_s = 0.02$ ms, CI width
$a_{\tau_F} = 68.1$ m/s^2	0.80	0.051	0.81	0.050	0.80	0.052
$a_{\tau_F} = 17.1$ m/s^2	3.2×10^{-5}	3.6×10^{-6}	3.1×10^{-5}	3.4×10^{-6}	3.1×10^{-5}	3.5×10^{-6}

Downloaded by UC IRVINE on March 15, 2017 | http://arc.aiaa.org | DOI: 10.2514/1.J055276

Next, we consider the product of importance weights

$$P_L = \frac{P_{\text{target}}(\boldsymbol{A}_1, \boldsymbol{A}_2, \ldots, \boldsymbol{A}_N)}{P_{\text{modified}}(\boldsymbol{A}_1, \boldsymbol{A}_2, \ldots, \boldsymbol{A}_N)} = \prod_i \frac{\exp(-(\|\boldsymbol{A}_i\|^2/(8\tau_F/3t_s)a_{\tau_F}^2))}{\exp(-(\|\boldsymbol{A}_i - \boldsymbol{m}_i\|^2/(8\tau_F/3t_s)a_{\tau_F}^2))} \tag{19}$$

which tells us how much smaller or larger the overall probability of getting a particular sequence of $\boldsymbol{A}_i$ would be if we were sampling from the true stochastic PDF rather than the sampling PDF used in the present calculations. Then, any statistic $\langle F(\boldsymbol{A}_1, \boldsymbol{A}_2, \ldots, \boldsymbol{A}_N)\rangle$ with respect to the distribution P_{target} can be estimated based on samples from the modified sampling distribution P_{modified} as

$$\begin{aligned}\langle F(\boldsymbol{A}_1, \boldsymbol{A}_2, \ldots, \boldsymbol{A}_N)\rangle &\equiv \int F(\boldsymbol{a}_1, \boldsymbol{a}_2, \ldots, \boldsymbol{a}_N)\, \mathrm{d}P_{\text{target}} \\ &= \int F(\boldsymbol{a}_1, \boldsymbol{a}_2, \ldots, \boldsymbol{a}_N) \frac{P_{\text{target}}}{P_{\text{modified}}}\, \mathrm{d}P_{\text{modified}} \\ &\approx \frac{1}{N_{\text{samples}}} \sum_{P_{\text{modified}}} P_L \cdot F(\boldsymbol{A}_1, \boldsymbol{A}_2, \ldots, \boldsymbol{A}_N)\end{aligned} \tag{20}$$

where we use $\mathrm{d}P_{\text{modified}}$ and $\mathrm{d}P_{\text{target}}$ to denote integration over the probability measures defined by the PDFs P_{modified} and P_{target}, respectively.

The particular statistic that we want to analyze in this work is the probability of growth to an instability:

$$P_{\text{growth}} = \int \chi_{\text{growth}}(\boldsymbol{a}_1, \boldsymbol{a}_2, \ldots, \boldsymbol{a}_N)\, \mathrm{d}P_{\text{target}} \tag{21}$$

where $\chi_{\text{growth}}(\boldsymbol{a}_1, \boldsymbol{a}_2, \ldots, \boldsymbol{a}_N)$ is the indicator function for a sample $(\boldsymbol{a}_1, \boldsymbol{a}_2, \ldots, \boldsymbol{a}_N)$ that exhibits growth (defined as increasing acoustic energy at the end of the simulation). Then, Eq. (21) gives the estimate

$$P_{\text{growth}} = \frac{\sum \chi_{\text{growth}} P_L}{N_{\text{samples}}} \tag{22}$$

In the present simulations, the samples from P_{modified} are used, which lead to instability much more often than the samples from P_{target}, but their importance weights are smaller, thus resulting in the correct calculation of the overall probability of instability via Eq. (21).

We next discuss the choice of $\boldsymbol{m}_i$ in Eq. (15). The $\boldsymbol{m}_i$ are best chosen so that the modified sampling distribution generates many samples that grow to instability. To do this, we introduce a simple control mechanism for the choice of $\boldsymbol{m}_i$ based on previous knowledge of the behavior of the combustion chamber. Specifically, from Sirignano and Popov [2] and Popov et al. [8], it is known that the 10-injector combustion chamber develops an acoustic instability in the shape of a first tangential acoustic mode for the cylindrical chamber and that perturbations in the shape of a first tangential mode will grow if their amplitude is greater than 20 atm.

We denote $\boldsymbol{P}(t)$ to be the coefficient of the first tangential mode in the order-one Bessel function expansion of $p(\boldsymbol{x}, t) - p_0$, where p_0 is the initial steady-state pressure, and we denote $\dot{\boldsymbol{P}}(t)$ to be the rate of change of $\boldsymbol{P}(t)$. Based on Eqs. (3) and (4), a simple model for the effect of acceleration on the evolution of $\boldsymbol{P}(t)$ and $\dot{\boldsymbol{P}}(t)$ is that $\boldsymbol{a}^C$ is a source term (but definitely not the only one), which contributes to the rate of change of $\dot{\boldsymbol{P}}(t)$:

$$\frac{\mathrm{d}\dot{\boldsymbol{P}}(t)}{\mathrm{d}t} = \langle \text{nonacceleration terms}\rangle + \frac{\rho a^2}{R}\boldsymbol{a}^C \tag{23}$$

Note that the preceding equation is a model that is only required to provide a good guess as to which $\boldsymbol{m}_i$ causes an increase in the oscillation amplitude; provided variance reduction is attained, the choice of $\boldsymbol{m}_i$ is inconsequential for the final probability prediction, as the importance sampling process removes the effect of the modified PDF. However, an appropriate choice for $\boldsymbol{m}_i$ can considerably increase computational efficiency. We make no claims to the exactness of this model but, as we shall see later, it is effective in its purpose.

To increase $\boldsymbol{P}(t)$, an appropriate choice for the mean of the modified distribution $\boldsymbol{m}_i$ is to take a vector that is in the direction of $\dot{\boldsymbol{P}}(t)$. More specifically, we take

$$\boldsymbol{m}_i = \frac{2\ \text{m/s}^2}{\text{atm}} \frac{\dot{\boldsymbol{P}}_{i-1}}{\|\dot{\boldsymbol{P}}_{i-1}\|} \times \max(20\ \text{atm} - \|\boldsymbol{P}_{i-1}\|, 0) \times \frac{20\ \text{ms}}{21\ \text{ms} - t_i} \tag{24}$$

that, provided that $\boldsymbol{P}_{i-1}$ has not grown above 20 atm, sets a bias in the realization of the acceleration time history that drives $\dot{\boldsymbol{P}}$ to increase in amplitude.

In particular, the direction of $\dot{\boldsymbol{P}}$ will be close to the direction of $\dot{\boldsymbol{P}}_{i-1}$ for the time interval $[t_{i-1}, t_i]$ because the length of that time interval is small (about 1/50th) when compared to the acoustic oscillation period of the chamber. Therefore, as the modified distribution will yield an $\boldsymbol{a}^C$ that is biased in the direction of $\boldsymbol{m}_i$, and hence $\dot{\boldsymbol{P}}$, the source term on the right-hand side of Eq. (23) will have a bias proportional to

$$\max(20\ \text{atm} - \|\boldsymbol{P}_{i-1}\|, 0) \times \frac{20\ \text{ms}}{21\ \text{ms} - t_i}$$

toward increasing the amplitude of $\dot{\boldsymbol{P}}$. The factors $\max(20\ \text{atm} - \|\boldsymbol{P}_{i-1}\|, 0)$ and $(20\ \text{ms}/21\ \text{ms} - t_i)$ are designed to bias the modified distribution away from samples that have a small pressure amplitude (the first factor) late in the simulation (the second factor) because those samples are unlikely to lead to an instability.

With the aforementioned definitions of the various components of the importance sampling procedure given, its operation in the context of an acoustic instability simulation is as follows:

1) If the time step is between t_{i-1} and t_i, two endpoints of one of the N intervals evaluate $\boldsymbol{a}^C$ according to Eq. (7) and use its value in the wave equations.

2) If the time step has just reached t_i, a) calculate $\boldsymbol{P}_i$, the coefficient of the first tangential mode in the order-one Bessel function expansion of $p(\boldsymbol{x}, t) - p_0$; b) approximate $\dot{\boldsymbol{P}}_i \approx (\boldsymbol{P}_i - \boldsymbol{P}_{i-1}/t_s)$, where t_s is the length of the time interval between t_{i+1} and t_i; c) substitute $\dot{\boldsymbol{P}}_i$, $\boldsymbol{P}_i$, and t_i in Eq. (24) to obtain $\boldsymbol{m}_{i+1}$; d) sample the random vector $\boldsymbol{A}_{i+1}$ according to Eq. (15); and e) use $\boldsymbol{A}_{i+1}$, as well as the previously evaluated $\boldsymbol{A}_i$, for the duration of the interval $[t_i, t_{i+1}]$.

It should be noted that, in this particular application, the success of the importance sampling procedure hinges on the existence of Eq. (23), an ordinary differential equation (ODE) that, although not an accurate predictor for the long-term evolution of the acoustic wave, gives a good local-in-time approximation to the effect of acceleration on the acoustic wave's rate of growth. A similar first-order model for the forcing term's effect on the variable of interest would generally be necessary for any application of importance-sampling-based variance reduction to CFD simulations.

IV. Computational Results

The mechanism for the development of a tangential combustion instability was described in detail in [2,8]. As a brief explanation, the external acceleration creates a transverse acoustic wave within the combustion chamber, in large part due to the effect of acceleration on the pressure at the chamber walls [Eq. (4)]. This transverse acoustic wave leads to oscillations in the heat release of combustion [2], via the effects of pressure on the reaction rate, as well as oscillations in the propellant mass flow at the injectors [6], due to a pressure wave propagating upstream in the injector ports. Finally, the oscillations in the heat release of combustion feed back into the pressure wave via the second term on the right-hand side of Eq. (2), causing growth of the pressure wave. An example of a growing acoustic instability due to transverse acceleration is shown in Fig. 3.

Next, we consider a disturbance with nominal rms value $a_{\tau_F} = 20.6\ \text{m/s}^2$ [corresponding via (13) to $\sigma_0 = 0.5\ \text{m/s}^{3/2}$], sampling interval $t_s = 0.01$ ms, and applied for $t_d = 20$ ms. The latter time

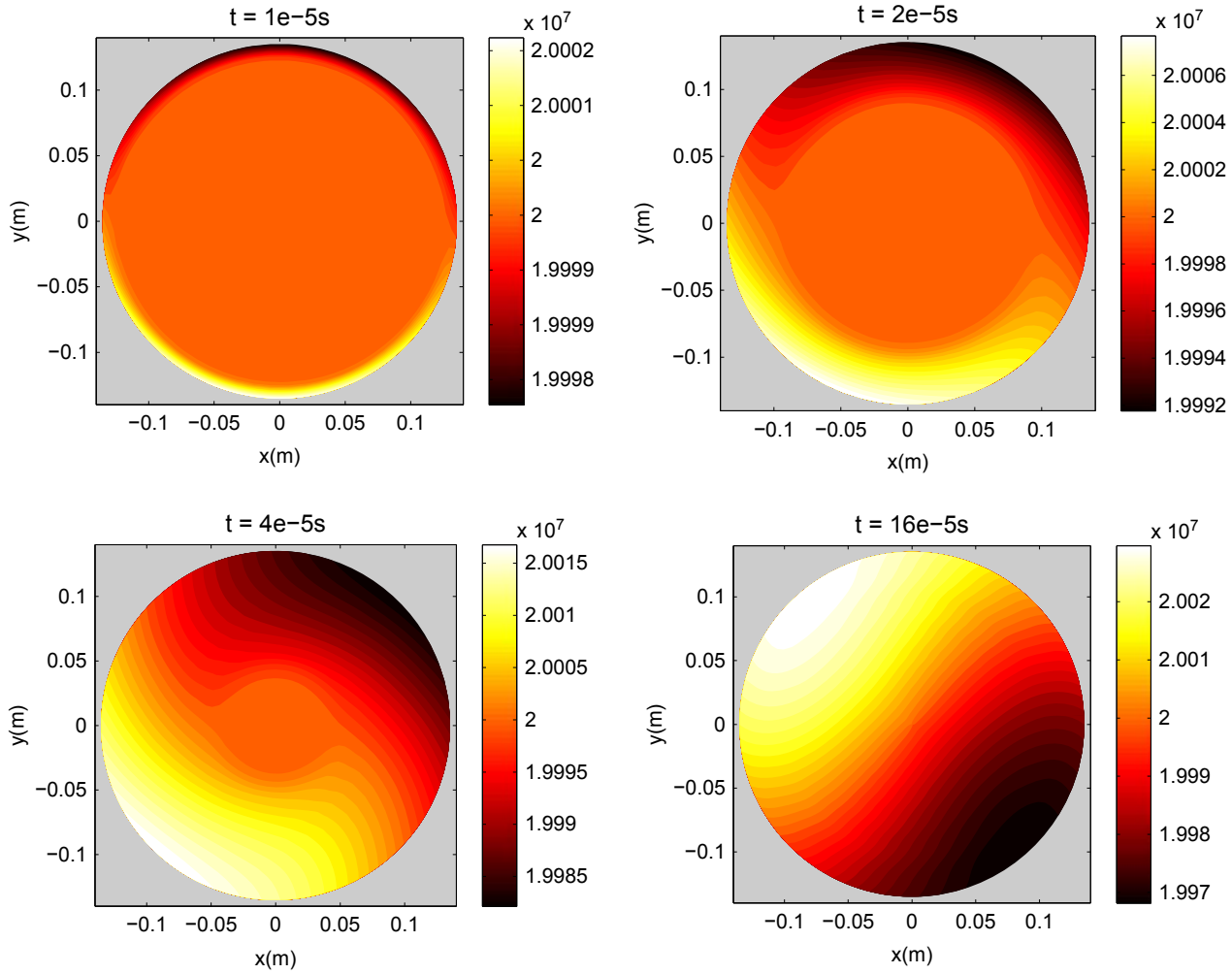

Fig. 3 Development of an acoustic instability due to transverse acceleration. Pressure perturbation is initiated at the chamber walls and propagates inward, establishing a spinning tangential wave.

interval is long enough when compared to the period of a first tangential mode $\tau_F = 0.453$ ms to allow detection of instability triggering. However, as discussed later in this section, the probability of triggering also depends on t_d. Using the importance sampling method outlined in the previous section, we derive a 95% confidence interval for the probability of growth to instability as follows:

$$P_{\text{growth}} \in [1.01 \times 10^{-4}; 1.22 \times 10^{-4}] \tag{25}$$

The variance reduction method outlined previously allows the calculation of this confidence interval based on only 2000 samples, of which approximately 37% yield growth to instability. To illustrate the vital contribution of the variance reduction procedure used here, we note that calculating this confidence interval using a standard Monte Carlo simulation would have required approximately four million samples.

This efficient variance reduction is, to a large part, due to the appropriate choice of the mean offsets in the modified distribution; to illustrate this, Fig. 4 plots the likelihood ratios generated by the modified distribution defined in Eq. (24), as well as the ratios generated by two simpler, but also inferior, choices for the mean offset.

In particular, the factor $\max(20 \text{ atm} - \|\boldsymbol{P}_{i-1}\|, 0)$ in Eq. (24) ensures that no unnecessary modifications in the sampling distribution are made for cases when the acoustic disturbance is already close to the critical threshold of 20 atm. This keeps the distribution of the likelihood ratios well conditioned; if a simple factor of 20 atm was used (alternative distribution 1, as shown in Fig. 4), the ratio of the highest to the lowest likelihood ratios would be much larger, leading to a wider confidence interval [6.2×10^{-5} instead of the 2.1×10^{-5} achieved with Eq. (24)].

On the other hand, the last term, $(20 \text{ ms}/(21 \text{ ms} - t_i))$ ensures that samples that remain at a low acoustic perturbation level late in the simulation receive a stronger push toward instability: this increases the total number of samples that achieve instability. Omitting this term (alternative distribution 2, as shown in Fig. 4) leads to a somewhat better conditioned likelihood ratios, but also a much lower number of samples that achieve instability, again leading to a wider confidence interval (9.7×10^{-5}).

Figure 5 shows a nongrowing sample and a growing sample, along time frequency components of the acceleration history that produced each one. As can be seen, the growing realization has a spike at the frequency of 2277 Hz, which is close to the first tangential frequency of 2202 Hz.

The previous results are obtained for $t_s = 0.01$ ms and $a_{\tau_F} = 20.6$ m/s^2. In Table 1, we present corresponding results for $t_s = 0.02$ and 0.05 ms to validate numerically the approximation of the target white noise signal by $a^C(t)$ in Eq. (7). As can be seen, fixing a_{τ_F} (equivalently σ_0) and varying t_s does not lead to a change in the probability of growth (the confidence intervals overlap).

Figure 5 provides evidence that the spectral content of the disturbance signal $a_x^C(t)$ at ω_F, which is the first-tangential-mode frequency, is closely connected to the triggering of instability.

Using the importance sampling procedure of Sec. III, we also explore the variation of the probability of growth to instability as a function of the asymptotically ($t_s \to 0$) expected rms acceleration a_{τ_F}. Figure 6 shows this probability, as a function of a_{τ_F}. For very large a_{τ_F}, the probability is practically one, which agrees with the

Downloaded by UC IRVINE on March 15, 2017 | http://arc.aiaa.org | DOI: 10.2514/1.J055276

Downloaded by UC IRVINE on March 15, 2017 | http://arc.aiaa.org | DOI: 10.2514/1.J055276

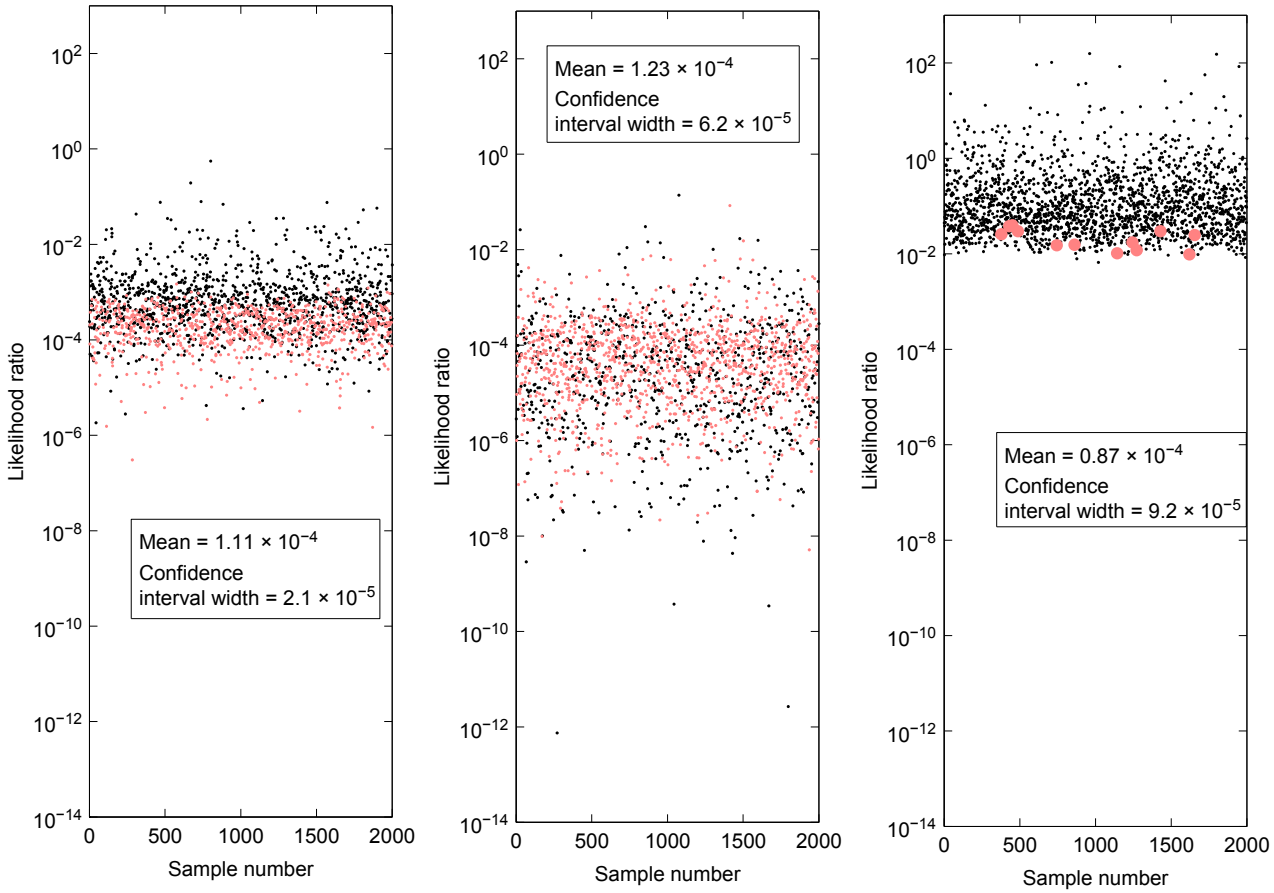

a) Modified distribution b) Alternative distribution 1 c) Alternative distribution 2

Fig. 4 Scatter plots of likelihood ratios for three different importance sampling distributions.

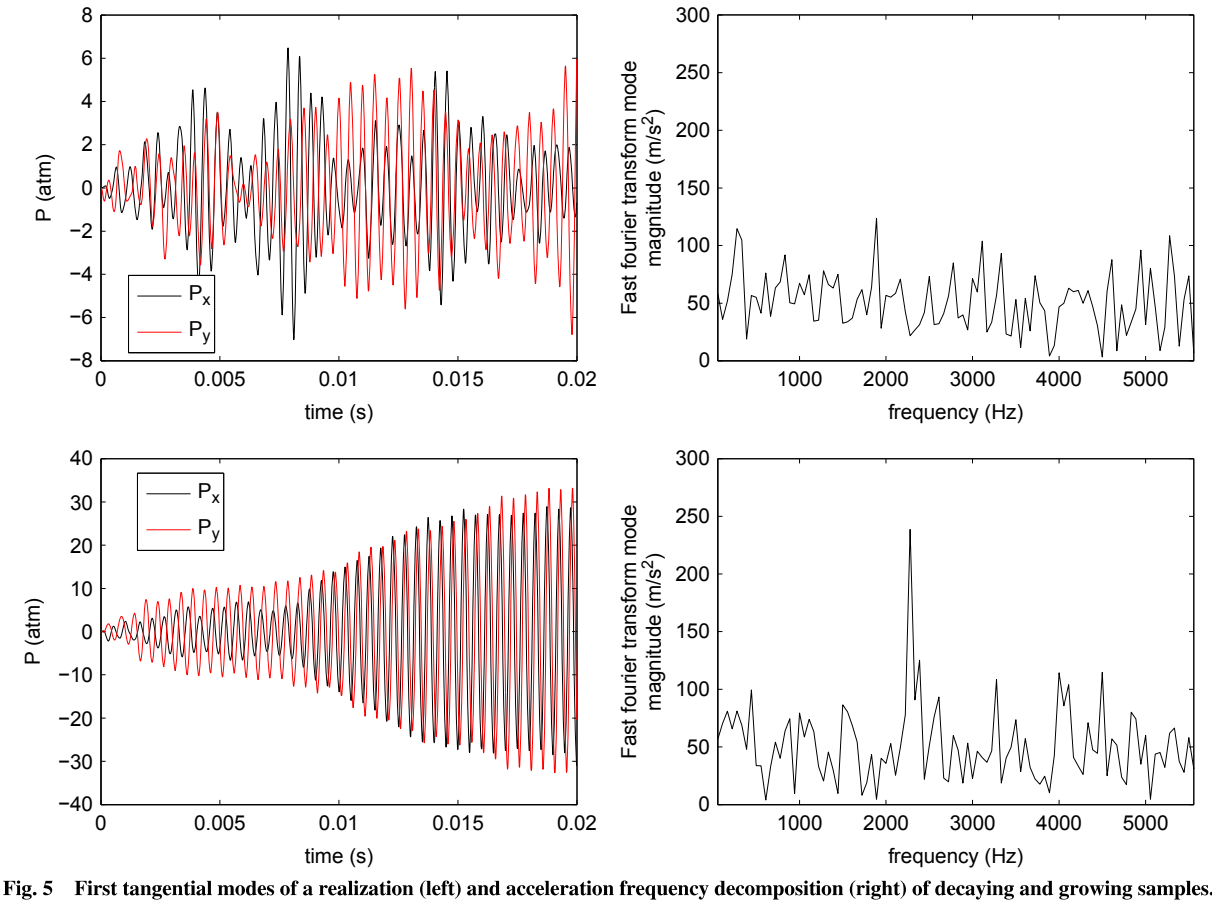

Fig. 5 First tangential modes of a realization (left) and acceleration frequency decomposition (right) of decaying and growing samples.

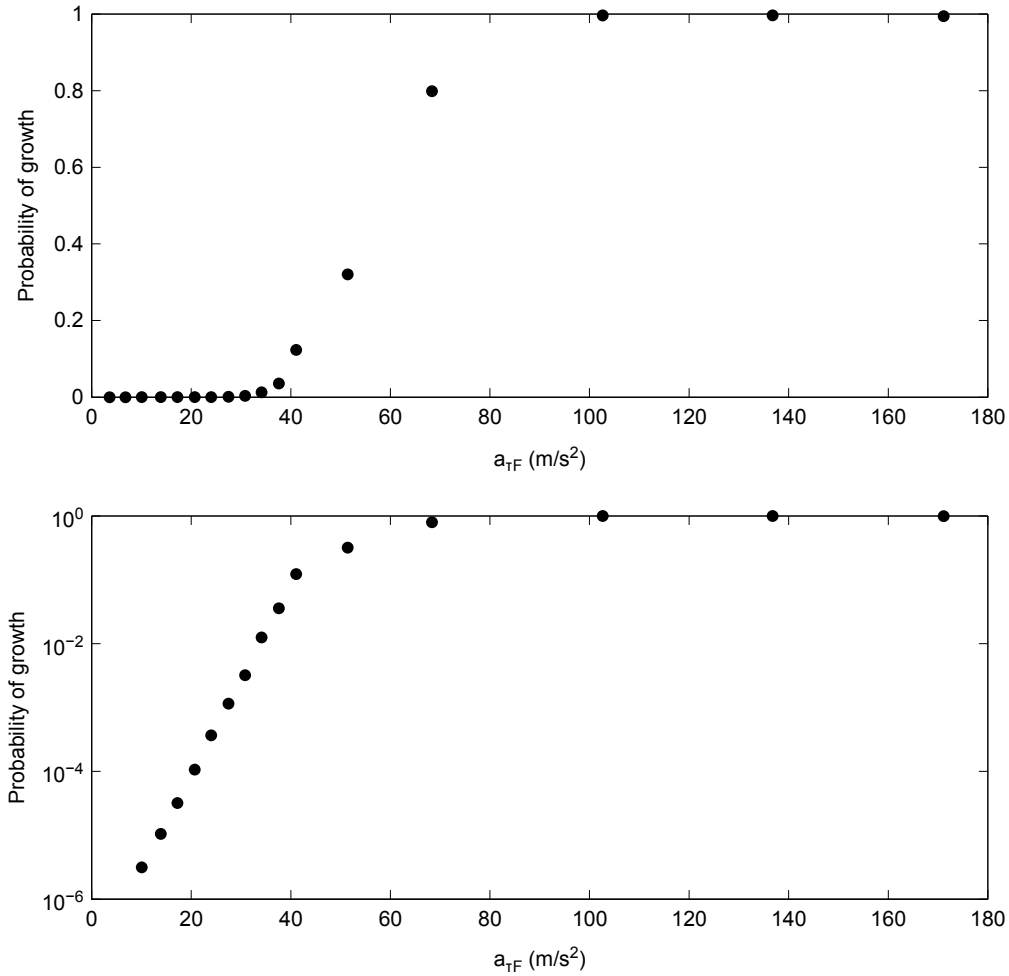

Fig. 6 Probabilities of growth to instability as a function of the expected rms amplitude a_{τ_F}: linear–linear plot (top), and log-linear plot (bottom).

findings of Popov et al. [8], where the authors were able to destabilize the motor using a pulse of magnitude of about 100 g and very short duration, equal to 1/20th of the value used here. On the log-normal version of that plot, we can also see that, for the intermediate range of a_{τ_F}, the probability of growth to instability increases in an approximately exponential fashion, with a 10-fold increase in growth probability caused by an approximately 7 m/s^2 increase in a_{τ_F}.

Another important parameter influencing the overall probability of growth is the total length in time of the acceleration disturbance. This is explored in Fig. 7, which plots the overall probability of growth versus the disturbance duration t_d for disturbances that are allowed to vary between the original length of $t_d = 20$ and 80 ms, as well as for a_{τ_F} values of both 13.7 and 34.3 m/s^2. A longer duration of the disturbance increases the probability of instability onset, but nowhere near as much as a larger rms amplitude a_{τ_F}: in particular, the probability of growth for $a_{\tau_F} = 13.7$ m/s^2, even with the quadrupled duration of 80 ms, is still lower than the probability of growth for the $a_{\tau_F} = 34.3$ m/s^2 pulse duration of 20 ms. On the right-hand side of Fig. 7, it can be seen that the data points follow the asymptotic trend $P_{\text{growth}} \sim A\exp(Bt^{1/2})$.

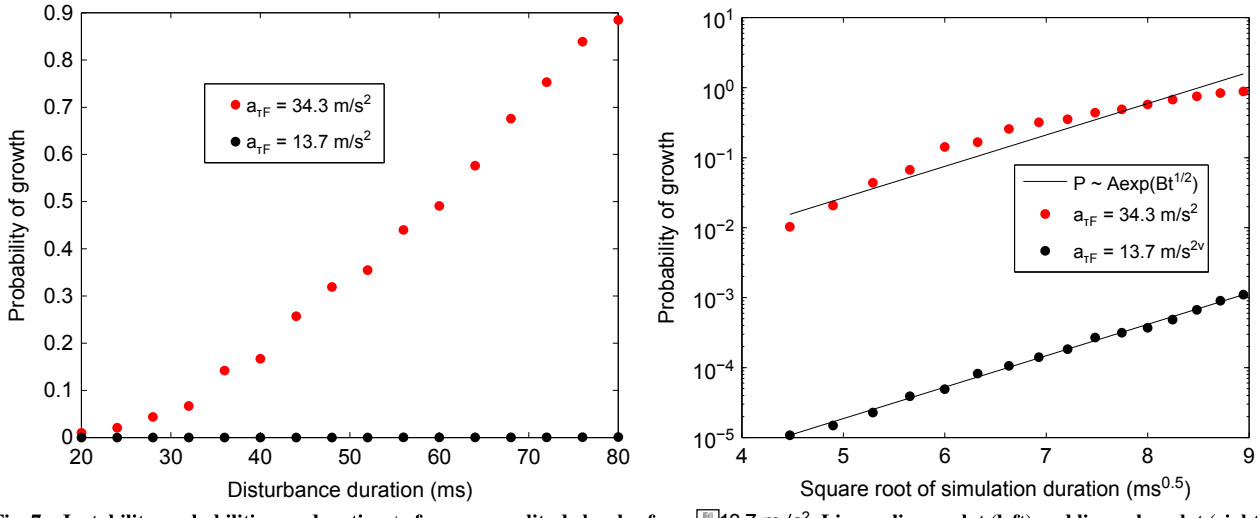

Fig. 7 Instability probabilities vs. duration t_d for rms amplitude levels of a_{τ_F} 13.7 m/s^2. Linear–linear plot (left) and linear-log plot (right).

Downloaded by UC IRVINE on March 15, 2017 | http://arc.aiaa.org | DOI: 10.2514/1.J055276

Additionally, Fig. 6 shows that, for rms amplitudes below 0.17 m/s^2, the probability of growth to instability is zero, at least within the stochastic accuracy of the present procedure: no realizations grew to instability. This is consistent with the fact that the motor itself is conditionally unstable so that small-amplitude disturbances decay. Disturbances caused by an acceleration history of rms 0.17 m/s^2 cannot accumulate quickly enough to outpace the damping within the chamber; thus, the critical amplitude above which a disturbance grows spontaneously will never be exceeded. To confirm this, a nonrandom acceleration of rms amplitude 0.17 m/s^2 and a sinusoidal wave pattern with a frequency matching that of the first tangential mode was tested and failed to produce an instability; the outcome is seen in Fig. 8. Because this type of disturbance is most likely to cause the growth of a first-tangential-mode pressure wave above the critical threshold, it is not surprising that the less coherent time histories also fail. Previous work has shown that a properly organized acceleration pulse of $O(1000\ \text{m/s}^2)$ applied for a short-duration [i.e., $O(1\ \text{ms})$] can exceed some physical threshold, and thereby trigger growth to a limit-cycle oscillation. Now, we see that substantially smaller-magnitude [i.e., $O(10\ \text{m/s}^2)$] random

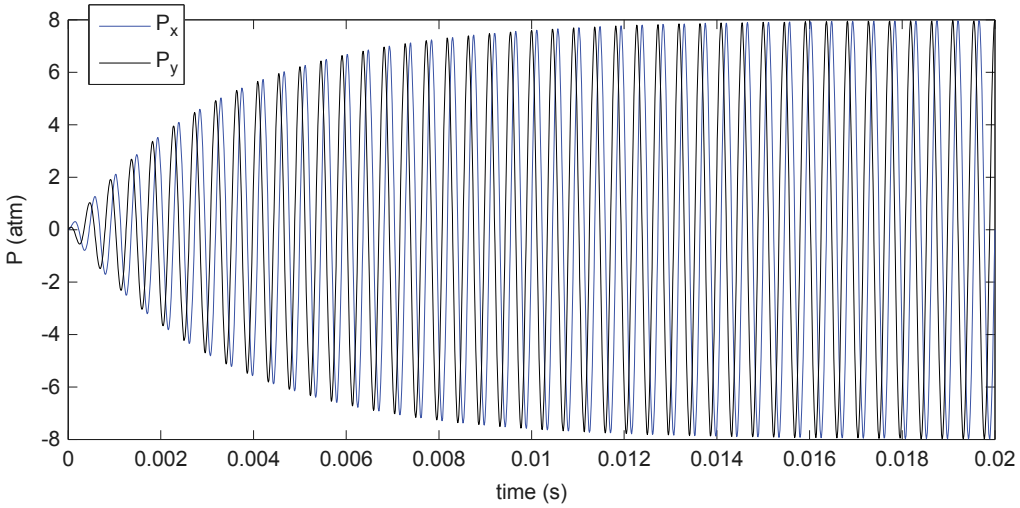

Fig. 8 Time response, given in terms of the P_x and P_y coefficients, of the acceleration time history a 6.9 m/s^2 $\hat{i}$ cos 2πt/τ_F 6.9 m/s^2 $\hat{j}$ sin 2πt/τ_F

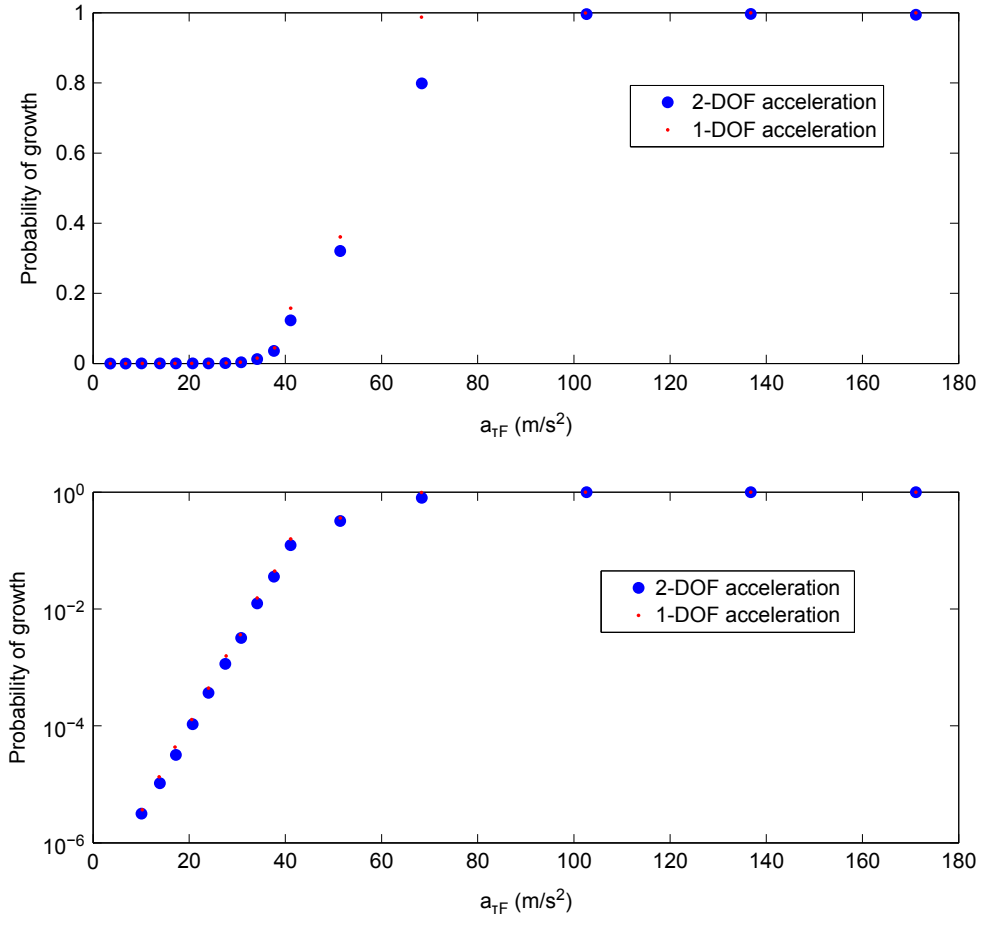

Fig. 9 Probabilities of instability vs. expected rms amplitude a_{τ_F}, for one- and two-degree of freedom acceleration time histories.

Downloaded by UC IRVINE on March 15, 2017 | http://arc.aiaa.org | DOI: 10.2514/1.J055276

vibration noise persisting for tens of milliseconds can, albeit with very small probability, trigger growth to the same limit cycle. Physically, there is a possibility that the random noise will include a sequence of small but properly directed pulses that collectively provide the forcing to exceed the threshold for triggering. As noted in Eq. (9), the key factor is the product of the duration of the noise and the square of the rms acceleration.

Finally, Fig. 9 makes a comparison between probabilities of growth to an instability when the acceleration has two degrees of freedom (in both the x and y directions, as we have been testing so far) and when the acceleration is constrained to the x direction only. As can be seen in the figure, for the same expected rms of acceleration, constraining the motion to the x direction only increases the probability of instability. This can be explained by the fact that a more constrained motion is more likely to contain coherent periodic components that can trigger an instability.

V. Conclusions

A new variance reduction method is proposed for the estimation of rare instability events in a liquid-propellant rocket engine. A modified distribution for the acceleration probability, with a higher than real likelihood of triggering rocket combustion instability, is introduced. The likelihood ratio is known and allows the low-cost modified distribution to yield the actual probability in a simple manner. Using an importance sampling scheme coupled with a simplified ordinary differential equation model for the evolution of the first tangential acoustic mode of the chamber, an accurate confidence interval for probabilities on the order of 1/10,000 can be obtained from 2000 samples, whereas without variance reduction, the number of samples required to obtain a similar confidence interval would be on the order of four million. Although the present study uses acceleration as the triggering mechanism for the rare-event instabilities, the present variance reduction method can be extended to other triggering mechanisms. Results show that the samples that grow are those in which the random acceleration time history has a large frequency spike near the frequency corresponding to the first tangential acoustic mode of the chamber. It is found that a random acceleration in one direction only produces a larger probability of growth for a given rms a_{τ_F} than a two-dimensional random acceleration. For moderate amplitudes of the rms acceleration a_{τ_F}, the probability of growth to instability increases exponentially with rising a_{τ_F}, and there is a critical threshold for a_{τ_F} below which no instability is triggered. Although this analysis uses engine acceleration as the trigger, previous works [2,6,7] have shown that other triggers can occur, and the limit cycle is independent of the triggering mechanism; thus, it is expected that those mechanisms or a combination of those mechanisms can also lead to a rare-event instability regime.

Downloaded by UC IRVINE on March 15, 2017 | http://arc.aiaa.org | DOI: 10.2514/1.J055276

Appendix: Computation of the Power Spectral Density of the Acceleration Disturbance

In this Appendix, we show analytically that, as $t_s \to 0$, $a_x^C(t)$ converges to white noise under the scaling law [Eq. (9)] by explicitly computing its power spectral density $\mathsf{S}_a(\omega; t_s)$ and showing that

$$\lim_{t_s \to 0} \mathsf{S}_a(\omega; t_s) = \sigma_0^2$$

which is a constant independent of frequency. To this end, we first express the Fourier transform of $a_x^C(t)$:

$$\mathsf{A}_x(j\omega) = \int_0^{t_d} a_x^C(t) e^{j\omega t}\, \mathrm{d}t = \sum_{i=0}^{N-1} \int_{t_i}^{t_{i+1}} a_x^C(t) e^{j\omega t}\, \mathrm{d}t \tag{A1}$$

Then, by substituting Eq. (A7) in Eq. (A1) and analytically computing the resulting integrals, we obtain

$$\mathsf{A}_x(j\omega) = j(\tau_1 + \tau_2 e^{j\omega t_s}) \cdot W - j(\tau_1 e^{j\omega t_s} + \tau_2) \cdot V \tag{A2}$$

where we introduce the expressions

$$\tau_1 \equiv \frac{2\omega^2 t_s^2 - \pi^2}{2\omega(\omega^2 t_s^2 - \pi^2)} \quad \text{and} \quad \tau_2 \equiv \frac{\pi^2}{2\omega(\omega^2 t_s^2 - \pi^2)} \tag{A3}$$

and the random variables

$$W \equiv \sum_{i=0}^{N-1} \boldsymbol{A}_i e^{j\omega t_i} \quad \text{and} \quad V \equiv \sum_{i=0}^{N-1} \boldsymbol{A}_{i+1} e^{j\omega t_i} \tag{A4}$$

Then, Eq. (A2) yields

$$\begin{aligned} E[|\mathsf{A}_x(j\omega)|^2] &= E[\mathsf{A}_x(j\omega) \cdot \mathsf{A}_x(j\omega)^*] \\ &= (\tau_1 + \tau_2 e^{j\omega t_s})(\tau_1 + \tau_2 e^{-j\omega t_s}) E[WW^*] \\ &\quad + (\tau_1 e^{j\omega t_s} + \tau_2)(\tau_1 e^{-j\omega t_s} + \tau_2) E[VV^*] \\ &\quad - 2\mathrm{Real}\{(\tau_1 + \tau_2 e^{j\omega t_s})(\tau_1 e^{-j\omega t_s} + \tau_2) E[WV^*]\} \end{aligned} \tag{A5}$$

Furthermore, from Eq. (A4), and using the assumed relations $E[\boldsymbol{A}_i \cdot A_k] = \sigma^2 \cdot \delta_{ik}$ ($\delta_{ik} = 1$ for $i = k$ and zero otherwise), we can easily compute

$$E[WW^*] = E[VV^*] = \sigma^2 \cdot N \quad \text{and} \quad E[WV^*] = e^{j\omega t_s} \sigma^2 (N - 1) \tag{A6}$$

and substituting Eq. (A6) and $N = t_d/t_s$ in Eq. (A5) gives an exact expression for the power spectral density of $a_x^C(t)$ as

$$\begin{aligned} \mathsf{S}_a(\omega; t_s) &= \lim_{t_d \to \infty} \left\{ \frac{1}{t_d} E[|\mathsf{A}_x(j\omega)|^2] \right\} \\ &= \lim_{t_d \to \infty} \frac{1}{t_d} \left[\frac{2\sigma^2 t_d}{t_s} \tau_2^2 (1 - \cos(2\omega t_s)) \right. \\ &\quad \left. + 2\sigma^2 (\tau_1^2 + \tau_2^2 \cos(2\omega t_s) + 2\tau_1 \tau_2 \cos(\omega t_s)) \right] \end{aligned} \tag{A7}$$

$$= \frac{2\sigma^2}{t_s} \tau_2^2 (1 - \cos(2\omega t_s)) \tag{A8}$$

because the second term inside the brackets in Eq. (A7) is bounded for fixed t_s and fixed ω. Next, substituting σ from Eq. (9) and τ_2 from Eq. (A3) in Eq. (A8), as well as taking $t_s \to 0$ for fixed ω, yields the desired result

$$\begin{aligned} \mathsf{S}_a(\omega; t_s = 0) \equiv \lim_{t_s \to 0} \mathsf{S}_a(\omega; t_s) = \lim_{t_s \to 0} \left\{ \frac{2\sigma_0^2}{t_s^2} \cdot \frac{\pi^4}{4\omega^2(\omega^2 t_s^2 - \pi^2)^2} \right. \\ \left. \cdot (1 - \cos(2\omega t_s)) \right\} = \sigma_0^2 \end{aligned} \tag{A9}$$

because, by L'Hospital's rule,

$$\lim_{t_s \to 0} (1 - \cos(2\omega t_s))/t_s^2 = 2\omega^2$$

Acknowledgments

This research was supported by the U.S. Air Force Office of Scientific Research under grant FA9550-15-1-0033, with Mitat Birkan as the Program Manager.

References

[1] Harrje, D., and Reardon, F., "Liquid Propellant Rocket Combustion Instability," NASA Rept. SP194, U.S. Government Printing Office, Washington, D.C., 1972.

[2] Sirignano, W. A., and Popov, P. P., "Two-Dimensional Model for Liquid-Rocket Transverse Combustion Instability," *AIAA Journal*,

Vol. 51, No. 12, 2013, pp. 2919–2934.
doi:10.2514/1.J052512
[3] Oefelein, J. C., and Yang, V., "Comprehensive Review of Liquid-Propellant Combustion Instabilities in F-1 Engines," *Journal of Propulsion and Power*, Vol. 9, No. 5, 1993, pp. 657–677.
doi:10.2514/3.23674
[4] Summerfield, M., "A Theory of Unstable Combustion in Liquid Propellant Rocket Motors," *Journal of the American Rocket Society*, Vol. 21, No. 6, p. 146, 1951.
doi:10.2514/8.4395
[5] Culick, F. E. C., "Unsteady Motions in Combustion Chambers for Propulsion Systems," *North Atlantic Treaty Organization*, AGARDograph AG-AVT-039, Neuilly-Sur-Seine, France, 2006.
[6] Popov, P. P., Sideris, A., and Sirignano, W. A., "Propellant Injector Influence on Liquid Propellant Rocket Engine Instability," *Journal of Propulsion and Power*, Vol. 31, No. 1, 2015, pp. 320–331.
doi:10.2514/1.B35400
[7] Popov, P. P., Sideris, A., and Sirignano, W. A., "Stochastic Modelling of Transverse Wave Instability in a Liquid Propellant Rocket Engine," *Journal of Fluid Mechanics*, Vol. 745, March 2014, pp. 62–91.
doi:10.1017/jfm.2014.96
[8] Popov, P. P., Sideris, A., and Sirignano, W. A., "Triggering and Restabilization of Combustion Instability with Rocket Motor Acceleration," *AIAA Journal*, Vol. 54, No. 5, 2016, pp. 1652–1659.
[9] Popov, P. P., and Sirignano, W. A., "Transverse Combustion Instability in a Rectangular Rocket Motor," *Journal of Propulsion and Power*, Vol. 32, No. 3, 2016, pp. 620–627.
doi:10.2514/1.B35868
[10] Crocco, L., and Cheng, S.-I., "Theory of Combustion Instability in Liquid Propellant Rocket Motors," AGARD Monograph 8, Butterworth, London, 1956.
[11] Crocco, L., and Sirignano, W. A., "Behavior of Supercritical Nozzle Under Three Dimensional Oscillatory Conditions," North Atlantic Treaty Organization, AGARDograph 117, Neuilly-Sur-Seine, France, 1967.
[12] Sirignano, W. A., and Krieg, J., "Two-Time-Variable Perturbation Theory for Liquid-Rocket Combustion Instability," *Journal of Propulsion and Power*, Vol. 32, No. 3, 2016, pp. 743–754.
doi:10.2514/1.B35953
[13] Swithenbank, J., and Sotter, G., "Vortex Generation in Solid Propellant Rocket," *AIAA Journal*, Vol. 2, No. 7, 1964, pp. 1297–1302.
doi:10.2514/3.2535
[14] Asmussen, S., and Glynn, P. W., *Stochastic Simulation: Algorithms and Analysis*, Springer, New York, 2007, pp. 126–138, 158–173.
[15] Glasserman, P., Heidelberger, P., and Shahabuddin, P., "Variance Reduction Techniques for Estimating Value-at-Risk," *Mathematical Finance*, Vol. 9, No. 2, 2002, pp. 117–152.
doi:10.1111/mafi.1999.9.issue-2
[16] Glasserman, P., "Tail Approximations for Portfolio Credit Risk," *Journal of Derivatives*, Vol. 12, No. 2, 2004, pp. 24–42.
doi:10.3905/jod.2004.450966
[17] Glynn, P., and Iglehart, D., "Importance Sampling for Stochastic Simulations," *Management Science*, Vol. 35, No. 11, 1989, pp. 1367–1392.
doi:10.1287/mnsc.35.11.1367
[18] Grundke, P., "Importance Sampling for Integrated Market and Portfolio Models," *European Journal of Operational Research*, Vol. 194, No. 1, 2009, pp. 206–226.
doi:10.1016/j.ejor.2007.12.028
[19] Arulampalam, S., Maskell, S., Gordon, N., and Clapp, T., "A Tutorial on Particle Filters for On-Line Non-Linear/Non-Gaussian Bayesian Tracking," *IEEE Transactions on Signal Processing*, Vol. 50, No. 2, pp. 174–188, 2002.
doi:10.1109/78.978374
[20] Pomeroy, B., "Measurement and Analysis of Combustor Response to Transverse Combustion Instability," Ph.D. Dissertation, Purdue Univ., West Lafayette, IN, 2012.
[21] Shipley, K., Morgan, C., Anderson, W., Harvazinski, M., and Sankaran, V., "Computational and Experimental Investigation of Transverse Combustion Instabilities," *Joint Propulsion Conference*, AIAA Paper 2013-3992, 2013.
[22] Gardiner, C. W., *Handbook of Stochastic Methods for Physics, Chemistry, and the Natural Sciences*, Springer–Verlag, Berlin, 1983, pp. 19–20.

T. L. Jackson
Associate Editor

Downloaded by UC IRVINE on March 15, 2017 | http://arc.aiaa.org | DOI: 10.2514/1.J055276